A SERS-Based Droplet Microfluidic Platform for Sensitive and High-Throughput Detection of Cancer Exosomes

Kwun Hei Willis Ho[1,#], Huang Lai[1,#], Ruolin Zhang[1], Haitian Chen[3,4], Wen Yin[1], Xijing Yan[2], Shu Xiao[1], Ching Ying Katherine Lam[1], Yutian Gu[1], JiaXiang Yan[1], Kunpeng Hu[2,*], Jingyu Shi[1,*], and Mo Yang[1,5.6.7,*]

[1] Department of Biomedical Engineering, The Hong Kong Polytechnic University, Kowloon, Hong Kong 999077, China

[2] Department of Breast and Thyroid Surgery, Lingnan Hospital, The Third Affiliated Hospital of Sun Yat-sen University, Guangzhou 510630, China

[3]Department of Hepatic Surgery and Liver Transplantation Center of The Third Affiliated Hospital of Sun Yat-sen University, Guangzhou 510630, China

[4]Organ Transplantation Research Center of Guangdong Province, Guangdong Province Engineering Laboratory for Transplantation Medicine; Guangzhou, 510630, China.

[5]The Hong Kong Polytechnic University Shenzhen Research Institute, Shenzhen 518000, China

[6]Joint Research Center of Biosensing and Precision Theranostics, The Hong Kong Polytechnic University, Kowloon, Hong Kong 999077, China

[7] Research Centre for Nanoscience and Nanotechnology, The Hong Kong Polytechnic University, Kowloon, Hong Kong 999077, China

Co-first author

* Corresponding authors: Kunpeng Hu: hukpeng@mail.sysu.edu.cn; Jingyu Shi: jing-yu.shi@polyu.edu.hk; Mo Yang: Mo.Yang@polyu.edu.hk

KEYWORDS: droplet microfluidics, surface-enhanced Raman spectroscopy, gold nanoparticles, exosome, cancer diagnosis

ABSTRACT

Exosomes, nanosized extracellular vesicles containing biomolecular cargo, are increasingly recognized as promising non-invasive biomarkers for cancer diagnosis, particularly for their role in carrying tumor-specific molecular information. Traditional methods for exosome detection face challenges of complexity, time consumption, and the need for sophisticated equipment. This study addresses these challenges by introducing a novel droplet microfluidic

platform integrated with a surface-enhanced Raman spectroscopy (SERS)-based aptasensor for the rapid and sensitive detection of HER2-positive exosomes from breast cancer cells. Our approach utilized an on-chip salt-induced gold nanoparticles (GNPs) aggregation process in the presence of HER2 aptamers and HER2-positive exosomes, enhancing the hot spot-based SERS signal amplification. This platform achieved a LOD of 4.5 $\log_{10}$ particles/mL with a sample-to-result time of 5 minutes per sample. Moreover, this platform has been successfully applied for HER2 status testing in clinical samples to distinguish HER2-positive breast cancer patients from HER2-negative breast cancer patients. High sensitivity, specificity, and the potential for high-throughput screening of specific tumor exosomes make this SERS-based droplet system a potential liquid biopsy technology for early cancer diagnosis.

Exosomes are 30-200 nm phospholipid vesicles containing DNA, RNA, lipids, metabolites, and proteins.[1] Exosomes are usually secreted by various of cells and present in most body fluids, including blood, urine, saliva, and breast milk, playing a crucial role in physiological and pathological processes.[2] Recent studies have shown that exosomes contain tumor-specific molecular information and have important roles in regulating the tumor microenvironment and tumor metastasis.[3-4] For example, exosomes derived from breast cancer cells in blood plasma exhibit overexpressed human epidermal growth factor 2 (HER2), which promotes tumor cell proliferation and accelerates disease progression.[5-6] Their abundance, easy accessibility, and high stability in body fluids make exosomes ideal non-invasive biomarkers for cancer diagnosis in liquid biopsy.[7-8] However, traditional exosome detection methods such as mass spectrometry,[9] enzyme-linked immunosorbent assay (ELISA),[10-11] and flow cytometry[12] require complex and time-consuming procedures and sophisticated equipment, limiting the feasibility of exosome detection for clinical use. Thus, there is an urgent need to develop rapid, high-performance, and convenient detection methods for tumor-specific exosomes.

Over the past decade, numerous biosensing techniques, including fluorescence,[13-14] colorimetric,[15] electrochemical,[16-17], and field effect transistor (FET),[18] have been utilized for rapid and sensitive detection of exosomes. Among them, surface-enhanced Raman scattering (SERS) has emerged as a promising tool due to its high sensitivity and fingerprint characteristics.[19,20] SERS offers inherent advantages over fluorescence, including minimal photobleaching effects, broad excitation wavelength range, and multiplexing detection capability.[21] Typically, the SERS-based detection method for exosomes can be categorized into label-free and labelling approaches. While label-free approaches may lack sensitivity,[22-23]

labelling with plasmonic nanoparticles co-functionalized with Raman reporters and bioactive layers (e.g., antibodies and aptamers) can enhance signals but require additional labelling procedures for SERS substrates, limiting their applicability for large-scale screening.[24-26] Nevertheless, SERS instrumentation, often involving sophisticated laser sources and spectrometers, can be bulky, expensive, and require specialized training, which may restrict its use in resource-limited point-of-care (POC) settings.[27] Therefore, developing a portable and user-friendly SERS platform with simplified sample preparation techniques remains challenging in exosome detection.

Droplet-based microfluidics as a subcategory of microfluidics offers several advantages over traditional microfluidics, providing uniform, controllable, and ultra-small droplets with rapid generation.[28] These droplets act as individual microreactors, ensuring a contamination-free and interfering-free environment for sensitive biological reactions and minimizing sample dilution and loss, thus increasing detection accuracy.[29] The high-throughput nature of droplet microfluidics facilitates rapid screening and analysis of numerous individual samples, which is essential for clinical diagnostics.[30] Integrating droplet microfluidics with fingerprinted SERS enables reproducible, highly sensitive, and scalable detection of exosomes, making this approach a powerful tool for early cancer diagnosis.[31] Labeled SERS-based microdroplet systems have been used to enhance the performance of aptamer and antibody-based immunoassays.[32-35] However, all these studies require off-chip modification steps for SERS nanotags. These additional steps lead to significant reagent consumption and labor-intensive procedures, making them unsuitable for high-throughput and point-of-care (POC) diagnostics. Furthermore, to our knowledge, SERS-based microdroplet platforms have not yet been extended to exosome detection.

Herein, we developed a SERS-based droplet microfluidic platform based on on-chip salt-induced gold nanoparticle (GNP) aggregation and Raman tags labelling processes for detection of HER2-positive exosomes of breast tumor cells. Initially, individual droplets were generated containing exosomes, aptamers, and gold nanoparticles (GNPs) and then injected with salt/Raman tags. In the absence of target exosomes, the aptamer layer covered on the surface of GNPs could prevent the aggregation of GNPs in high-salt conditions, resulting in no change of SERS signal. In the presence of target exosomes, the HER2 aptamers will detach from GNPs due to higher affinity between aptamers and target exosomes, leading to GNP aggregation under high-salt conditions with SERS signal enhancement due to hot spots generation. By monitoring the change of SERS signals, we can sensitively and specifically detect Her2-positive exosomes derived from breast tumor cells with a LOD of 4.5 $\log_{10}$

particles/mL in biomimetic samples. Moreover, the diagnostics ability of this platform was also demonstrated in the plasma clinical samples of breast cancer patients for potential clinical applications. To the best of our knowledge, this is the first study that uses a simple SERS-based microdroplet platform with on-chip salt-induced GNP aggregation process and hot spot-based signal amplification for quantitative tumor exosome detection.

RESULTS AND DISCUSSION

Mechanism of SERS-based Droplet Microfluidic Platform for Detection of HER2-Positive Tumor Exosomes. The droplet-based microfluidic platform integrated with the SERS aptasensor consists of four main parts: the droplet generator, the salt/Raman tags microinjection section, the mixing section, and the SERS signal observation section (Figure 1). The first step was to inject a mixture of gold nanoparticles (GNPs), exosomes (Exo), and HER2 aptamers into the sample inlet, after which they were encapsulated within individual droplets at the droplet generation junction. Depending on the presence or absence of target exosomes, the droplets were classified as either target droplets (containing HER2-positive exosomes) or non-target droplets (lacking HER2-positive exosomes). In target droplets, HER2 aptamers specifically bind to the targeted HER2-positive transmembrane biomarker on the exosome surface, leaving the GNPs unprotected. But in non-target droplets, HER2 aptamers are absorbed on the surface of GNPs, acting as a protective layer to prevent the aggregaton of GNPs. Subsequently, the salt/Raman tags solution is injected into each droplet by a microelectrode-based injection unit in the microinjection section. Typically, in non-target droplets, the GNPs remain unaggregated due to the protective aptamer layer that ensures electrostatic repulsion. However, in the target droplets containing HER2-positive exosomes, the unprotected GNPs will aggregate together with the Raman tags after the injection of salt solution in the droplets, resulting in hot spot-enhanced SERS signals. The SERS signals of each droplet are then be measured when the droplets pass through the SERS detection zone under a 785 nm laser. By analyzing the SERS signals of each droplet, the target droplets with HER2-positive exosomes can be identified with enhanced SERS signals.

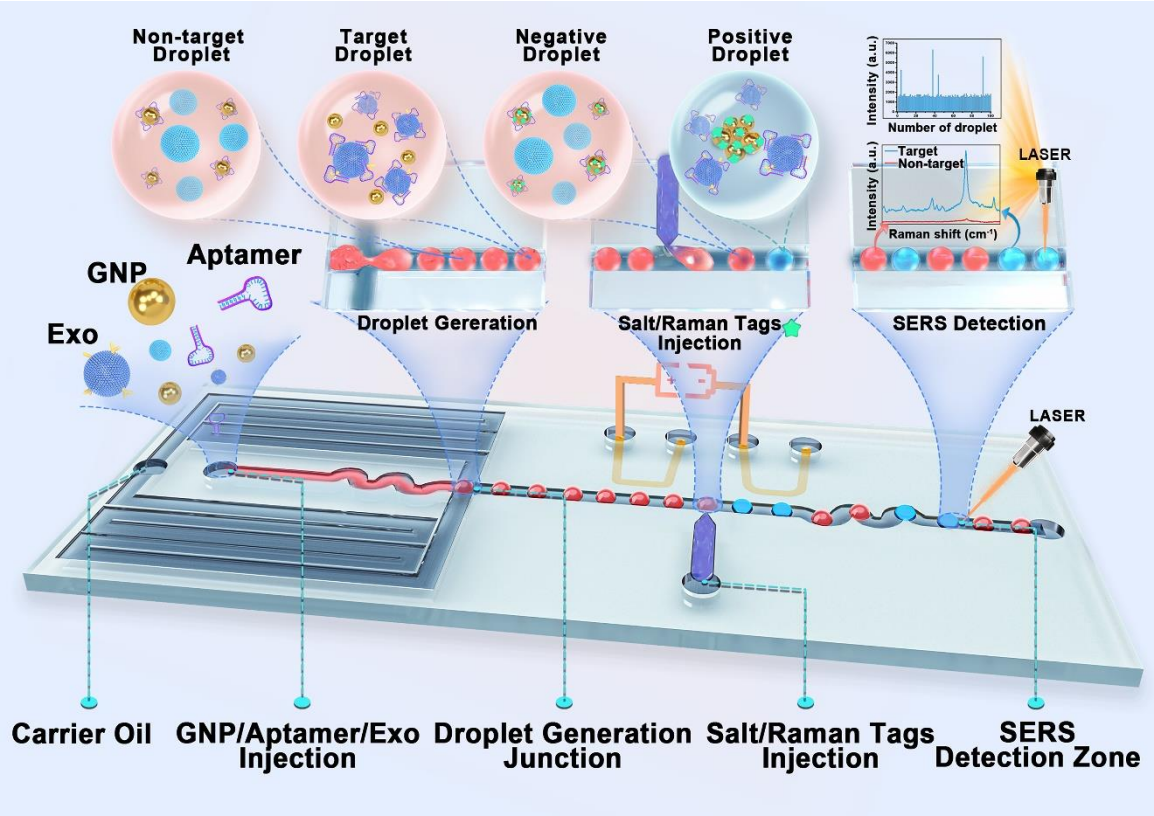

Figure 1. Illustration of the process of SERS-based droplet microfluidic platform for detecting HER2-positive tumor exosomes.

Characterization of Exosomes and GNPs

Three breast tumor cell lines of SKBR3, MCF-7, and MDA-MB-231 were used in the experiments, where SKBR3 represents HER2-positive breast tumor, and MCF-7, and MDA-MB-231 represent HER2-negative breast tumor. The morphology of exosomes from all three breast tumor cell lines showed membrane-bound structures with diameters of 130 nm, 163 nm, and 198 nm by TEM imaging, respectively (Figure 2a). The concentration and size distribution of exosomes were measured by a nanoparticle tracking analysis (NTA) system, and the results showed that the average particle size of exosomes from the three cell lines ranged from 100 nm to 200 nm, and the concentration was approximately 10.2 $\log_{10}$ particles/mL (Figure 2b). The membrane protein expression of exosomes was then explored using Western blotting. As shown in Figure 2c, SKBR3 cell-derived exosomes have significantly high levels of HER2 expression, which lays the foundation for the specific detection of exosomes using HER2 aptamers. Moreover, CD63 is the common exosome biomarker on the surface of all three types of exosomes, while HER2 and CD44 are overexpressed explicitly on the surface of SKBR3 exosomes and MDA-MB-231 exosomes, respectively. These findings were consistent with the other studies.[6, 36] GNPs were synthesized using a seed-mediated method according to previous

protocols.[37] TEM analysis confirmed that the GNPs had a good round shape with an average size around 15 nm (Figure 2d). After aptamer absorption, the size of GNP slightly increased from 15.5 nm to 17.5 nm (Figure S1) and GNP/HER2 aptamer complex showed an absorption peak at 260 nm, indicating the binding of aptamers on the GNP surface (Figure 2e). After the addition of HER2-expressed SKBR3 exosomes, an obvious decrease in the absorption peak at 260 nm of GNP/HER2 aptamer complex was observed, suggesting the detachment of HER2 aptamers from the GNP surface due to the specific binding interaction with target exosomes (Figure 2e). Dynamic light scattering (DLS) measurement also revealed a slight decrease in the hydrodynamic size of the GNP/HER2 aptamer complex, from 18 nm to 15.5 nm, which is similar to the size of bare GNPs (Figure 2f). Zeta potential measurement was used to characterize the surface charge screening phenomenon of GNPs before and after the salting process. The Zeta potentials of bare GNPs significantly increased from -26 mV to -10 mV under high concentrations of salt, which had the potential to diminish the electrostatic repulsion between GNPs, leading to their aggregation (Figure S2).

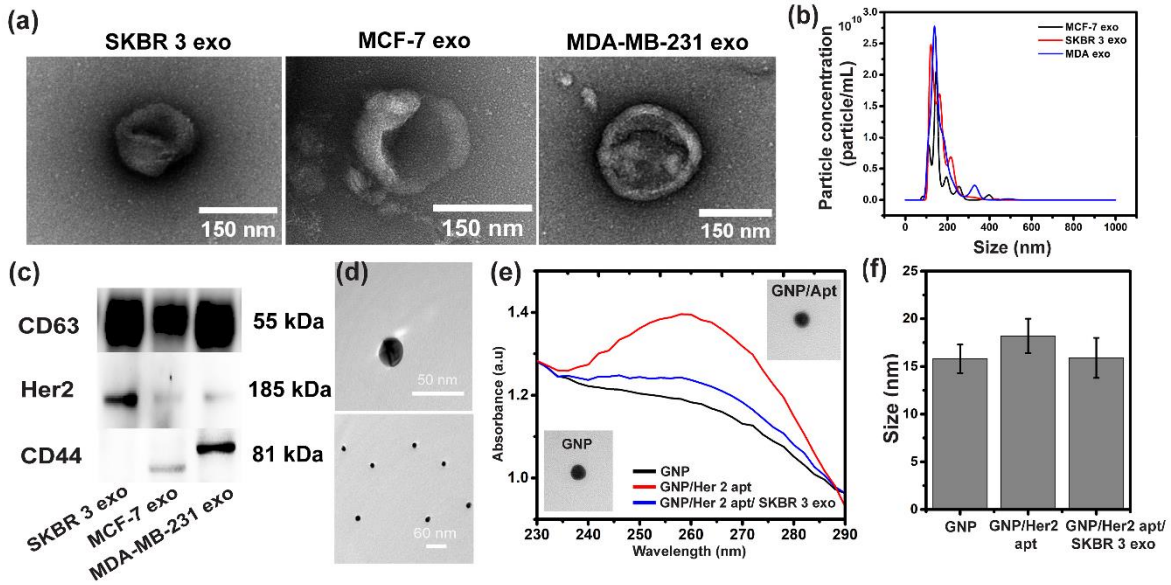

Figure 2. (a) Negative staining TEM images of cancer cell-derived exosomes from SKBR3, MCF-7, and MDA-MB-231 cell lines. (b) The size distribution of SKBR3 Exo, MCF-7 Exo, and MDA-MB-231 Exo was obtained by NTA. (c) Western blotting analysis of CD63, HER2, and CD44 proteins from the SKBR3 Exo, MCF-7 Exo, and MDA-MB-231 Exo. (d) TEM images of isolated bare GNPs. UV-vis absorbance spectra (e) and DLS measurement (f) of GNP, GNP/HER2 aptamer compex, and GNP/HER2 aptamer compex isolated after mixing with SKBR3 Exo. The absorption peak at 260 nm indicated

the aptamer absorption. All samples are washed 3 times to remove the excessive HER2 aptamers.

SERS-based Aptasensor for Detection of HER2-positive Exosomes

We hypothesized that the aggregation of GNPs would generate strong and increased plasmonic hot spots, thereby enhancing the SERS intensity of Raman tags due to the enhancement factor M_{total} being sensitive to the local field strength within the hot spots.[38] To prove our hypothesis, 5, 5'-dithiobis (2-nitrobenzoic acid) (DTNB, 2 µL, 3 µM) was used as Raman tags to maximize the SERS signal contrast pre- and post-GNP aggregation. During the salting process, DTNB molecules were incorporated into the vacancies on the GNP surface.[39] In the presence of target exosomes, the high-affinity interaction between aptamer and exosomes initiated salt-induced GNP aggregation, positioning Raman tags between plasmonic nanostructures and fostering the formation of more robust and increased hot spots, thereby amplifying SERS signals. Figure 3a illustrates a significant increase in the overall SERS spectra of this aptasensor upon salt and Raman labelling in the presence of SKBR3 exosomes, indicating the successful recognition of HER2-positive exosomes and consequent salt-induced GNP aggregation. The colorimetric measurement also showed a visible color change of GNPs from red to blue in the presence of SKBR3 exosomes, indicating the aggregation of GNPs (Figure S3). The peak of DTNB in the SERS spectrum is most prominent at 1339 cm^{-1}, which was selected as the characteristic peak for signal readout due to the symmetric stretching of the nitro group.[40]

Then, we investigated the sensitivity of the SERS-based aptasensor for HER2-positive exosomes. Figure 3b shows that the DTNB peak intensity increased as the concentration of SKBR3 exosomes increased from 3.5 $\log_{10}$ particles/mL to 7.5 $\log_{10}$ particles/mL. Based on the control signal plus three times the noise signal, the LOD of the SERS-based aptasensor was calculated to be 4.76 $\log_{10}$ particles/mL (Figure 3c). To test the specificity of this SERS-based aptasensor, we evaluated non-cancerous and HER2-negative exosomes as controls using different aptamers (e.g., CD63, HER2, and CD44 aptamers) (Table S1). When detecting SKBR3 exosomes, the DTNB-peak intensity of the aptasensor dramatically increased using CD63 and HER2 aptamers (Figure 3d, top). Conversely, when detecting non-cancerous exosomes, representative of exosomes from normal cells, the vigorous DTNB-peak intensity of the aptasensor was only observed using CD63 aptamers (Figure 3d, bottom). Interestingly, this aptasensor demonstrated strong SERS signals when detecting MDA-MB-231 exosomes with both CD63 and CD44 aptamers, whereas MCF-7 exosomes showed positive signals exclusively with CD63 aptamers (Figure S4). The concentration-dependent effects for detecting different exosomes were respectively investigated with increasing exosome concentrations from 3.5 to

7.5 $\log_{10}$ particles/mL using CD63, HER2, and CD44 aptamers (Figure S5). These findings not only underscored the high specificity of our SERS-based aptasensor for detecting SKBR3 exosomes but also demonstrated its versatility in adapting to various biomarkers for broader diagnostic applications.

To explain the improvement in detection sensitivity, we investigated GNP aggregation using TEM and the Finite-Difference Time-Domain (FDTD) method. TEM confirmed GNP aggregation, while FDTD simulations revealed that larger aggregates formed more plasmonic hot spots and significantly increased Raman enhancement factors due to interparticle coupling (Figure 3e). We calculated the average Raman enhancement factor for monomers, trimers, and pentamers as 21, 158, and 256, respectively (Figure S6). The results indicated that increased GNP aggregation led to more efficient light confinement and higher Raman signal enhancement, demonstrating the exceptional sensitivity of our SERS-based aptasensor for the detection of HER2-positive exosomes.

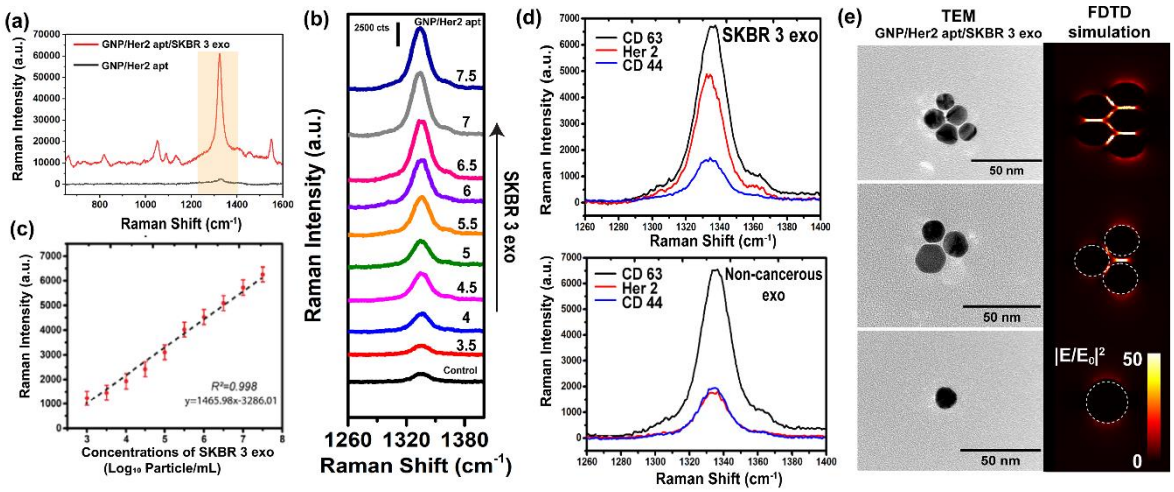

Figure 3. The SERS-based aptasensor for SKBR3 exosome detection using 5,5'-dithiobis (2-nitrobenzoic acid) (DNTB) as Raman tags. (a) The whole SERS spectra of the aptasensor in the presence of SKBR3 exosomes containing additional salt/DNTB. (b) The DTNB characteristic peak intensity at 1339 cm^{-1} of the aptasensor with increasing concentration of SKBR3 exosome from 3.5 to 7.5 $\log_{10}$ particle/mL. (c) Linearity evaluation of DTNB-peak intensity versus the concentration of SKBR3 exosome. (d) Selectivity study of the SERS-based aptasensor for SKBR3 exosome. The DTNB-peak intensity of the aptasensor for the detection of SKBR3 exosomes (top) and non-cancerous exosomes (bottom) using CD63, HER2, and CD44 aptamers, respectively. (e) TEM images of aggregated GNPs incubated with HER2 aptamer and SKBR3 exosome (Left). The corresponding Finite-Difference Time-Domain (FDTD) SERS enhancement simulation of GNP. The nanoparticle radius is set as 10 nm (Right).

Establishment and Optimization of the SERS-based Droplet Microfluidic Platform

To enhance sensitivity and throughput, we further integrated our SERS-based aptasensor with a droplet-based microfluidic platform to achieve automated, sensitive, and high-throughput detection of tumor exosomes. The fabrication of the droplet-based microfluidic platform adhered to the methodology outlined in our prior investigation.[29] The chip design encompassed four primary elements: a droplet generator, an electrode-induced microinjection zone, a curved mixing channel, and a droplet detection zone (Figure 4a). Typically, water-based single droplets containing aptamers, exosomes, and GNPs were generated at a water/oil flow-focusing junction (Figure S7), going through an injection zone where the Raman reporter DTNB and salt solution at fixed concentrations were injected with the assistance of an applied electric field (Figure 4b). The droplets then entered a curved mixing channel, inducing vortex flow that facilitated mixing for subsequent SERS signal measurement in the droplet detection zone. Based on the 785 nm laser-induced SERS detection system, HER2-positive tumor exosomes could be sensitively and rapidly detected within the droplet.

To confirm the effective encapsulation of exosomes within individual droplets, we utilized DiD Cell-Labeling dye for fluorescent labeling and observed the fluorescence signal within the droplets. Figure 4c showed that the fluorescence signals of the stained exosomes colocalized within the droplets, confirming successful encapsulation. We also examined the correlation between injection channel pressure and droplet volume to ensure the precise and stable injection of Raman tags and salt solution. It was observed that the droplet volume increased linearly with the increase of the jet channel pressure, particularly from 202.2 mbar to 204.9 mbar, which resulted in an increase in the droplet diameter from 49.3 to 58.5 μm (Figure 4d). The collected microdroplets exhibited uniform spherical size with <2% variation in radius, indicating high reproducibility of the droplet-based microfluidic channel. The injection concentration of the salt/Raman tag mixture was optimized to 0.5 M NaCl and 1mM DTNB at an injection channel pressure of 204.25 mbar, maximizing the SERS signal intensity of the droplets containing SKBR3 exo at 7 $\log_{10}$ particles/mL (Figure 4e). The concentration of NaCl and DTNB in each droplet was calculated to be 140 mM and 285 μM, respectively. This optimization demonstrated the capability of our platform to precisely control injection and fine-tune the Raman tag/salt solution concentrations in each droplet.

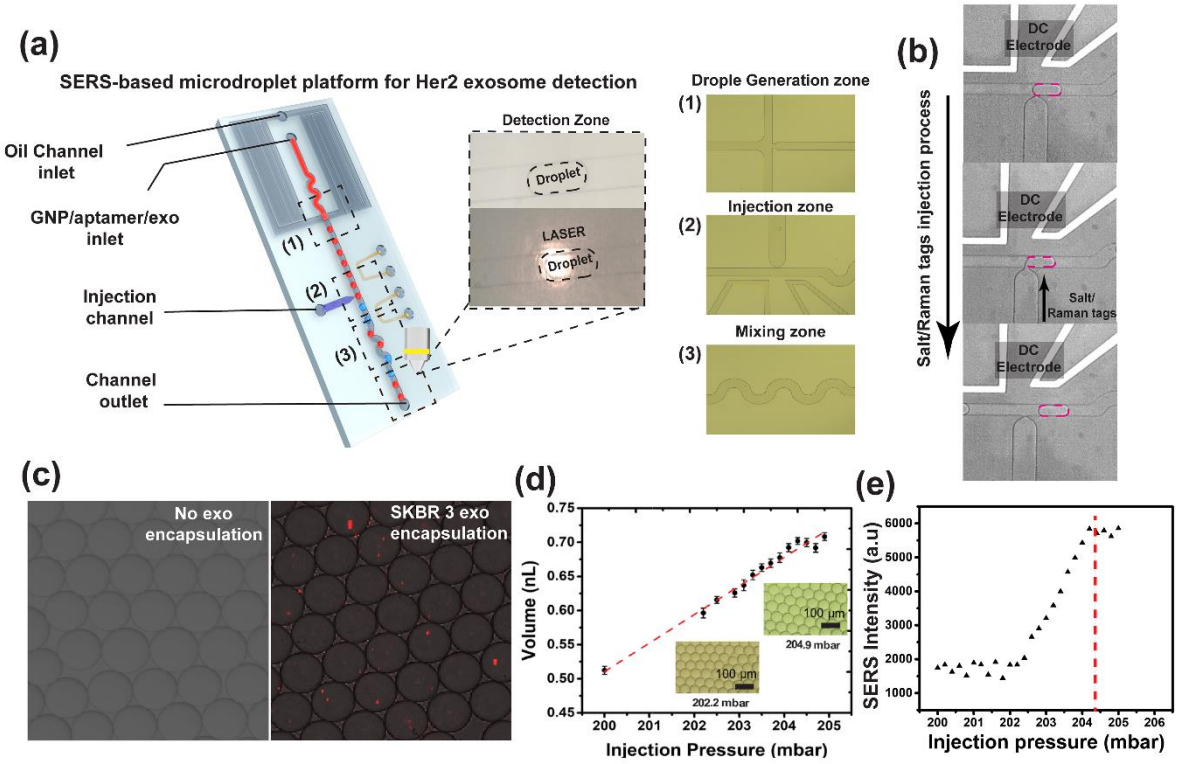

Figure 4. Establishment and optimization of the SERS-based microdroplet platform. (a) The structure and principle of the droplet based microfluidic chip integrated with SERS-based aptasensor for exosome detection. The optical microscope images show the detection zone with a focused LASER spot and the other parts of the droplet-based microfluidic chip, including (1) Droplet generation zone, (2) Salt/Raman tags injection zone, and (3) Mixing zone. (b) The electrode-assisted salt/Raman tags injection process. (c) The fluorescence image overlayed on a bright field image of the generated droplet. The SKBR 3 exo was labeled with DiD Cell-Labeling dye, and the exo concertation was fixed at 7 $\log_{10}$ particles/mL. (d) The droplet volume change (nL) under different applied pressures in the injection channel. (e) The SERS intensity collected from positive droplets under different injection pressures.

SERS-based Droplet Microfluidic Platform for Detection of Tumor Exosomes Derived from the Cell Line.

The optimized SERS-droplet microfluidic platform was used for sensitive and high-throughput detection of HER2-positive exosomes. The SERS-based aptasensor was encapsulated into single droplets and measured through continuous on-chip SERS signal readout under a 785 nm laser after the Nacl/Raman tags solution injection. The exposure time for each droplet was fixed at 0.5 seconds, ensuring consistent acquisition parameters. The background subtraction was applied to the collected DTNB-SERS signal at 1339 cm^{-1} to ensure data accuracy (Figure S8).

In negative droplets, the GNPs were expected to remain monodispersed due to the protective effect of the aptamer layer against salt, resulting in a weak SERS signal intensity. Conversely, in positive droplets, the strong binding affinity between HER2 aptamers and SKBR3 exosomes was expected to cause salt-induced aggregation of unprotected GNPs, generating hot spots and amplifying the SERS signal (Figure 5a). The SERS spectra and DTNB-peak intensities of the positive droplets were recorded and analyzed against increased concentrations of SKBR3 exosomes, ranging from 3.5 to 5.5 $\log_{10}$ particles/mL in Figure 5b and 5c, respectively. The limit of detection (LOD) was estimated to be 4.5 $\log_{10}$ particles/mL using the control signal plus three times the noise signal. To further compare this sensitivity with existing exosome detection methods, we used nano-flow cytometry to detect the SKBR3 exosomes with various concentrations. As shown in Figure S9, the nano-flow cytometry could only detect SKBR3 exosomes at concentrations around 8 $\log_{10}$ particles/mL, which was significantly higher than the LOD at 4.5 $\log_{10}$ of our SERS-droplet microfluidic platform. Moreover, the total detection time for nano-flow cytometry was more than 1.5 h, and it required sample pre-labeling and washing procedures, making it time-consuming and labor-intensive. However, our SERS-droplet microfluidic platform achieved a rapid sample-to-result time, estimated at 5 minutes per sample.

To test the specificity of the SERS-based microdroplet platform, we simulated clinical scenarios of mixture of SKBR3 and non-cancerous exosomes at different ratios (SKBR3: non-cancerous; 1:1, 1:10, $1:10^2$, $1:10^3$, $1:10^4$, $1:10^5$, $1:10^6$) to detect HER2-positive exosomes (Figure 5d). Here, the concentration of non-cancerous exosomes was fixed at 9.5 $\log_{10}$ particles/mL, while the concentration of SKBR3 exosome was decreased from 9.5 to 3.5 $\log_{10}$ particles/mL. The results showed that the presence of non-cancerous exosomes did not significantly affect the intensity of the HER2-positive signal. As the mixing ratio decreased, the signal intensity also decreased, which was consistent with the sensitivity study. Our SERS-based microdroplet platform could distinguish SKBR3 exosomes from non-cancerous exosomes at a ratio as low as $1:10^5$ (i.e. 0.001% of total exosomes) in the biomimetic samples.

To further investigate the screening capability of the SERS-based microdroplet platform, a comprehensive screening analysis of nanosensors based on 3 aptamers (CD44 apt, HER2 apt and CD63 apt) for exosomes from 4 cell-lines (non-cancerous, MCF-7, SKBR3, and MDA-MB-231) was conducted (Figure 5e). The same concentration at 5.5 $\log_{10}$ particles/mL was used for all the 4 types of exosomes during the experiments. As expected, nanosensors with HER2 apt could specifically detect droplets with SKBR3 exosomes and showed low signals for the other 3 types of exosomes in the screening plot. Moreover, nanosensors with CD44 apt could

specifically detect droplets with MDA-MB-231 exosomes and showed low signals for the other 3 types of exosomes. Finally, nanosensors with CD63 apt showed high signals for droplets with all the 4 types of exosomes since CD63 is the common exosome biomarker. The corresponding quantitative analysis of the collected SERS signal intensity from droplets is shown in Figure 5f. These findings revealed that our SERS-based microdroplet platform has the potential for rapid screening of variouis specific tumor exosomes by modifying the aptamers on the nanosensors.

Then, we simulated the screening process using different proportions of positive droplets and negative droplets. First, to establish the baseline for HER2 droplet screening, we conducted a statistical analysis by adding three standard deviations to the mean reference signal intensity of the HER2-negative droplets. Then, we mixed various ratios of SKBR3 exosome droplets with non-cancerous exosome droplets and measured the SERS intensity from 100 random droplets. Since each droplet only required 0.5 s of exposure time, the total measurement time for 100 droplets was 50 s. When the ratio of SKBR3 exosome droplet to non-cancerous exosome droplet was 10% to 90%, 9 spike signals (9%) were successfully recorded after 100 measurements, which closely mirrored the initial mixing ratio (10%) (Figure S10). When the ratio was reduced to 5% SKBR-3 exosome droplets to 95% non-cancerous exosome droplets, 4 spike signals (4%) were detected out of 100 droplets, again largely reflecting the initial mixing ratio (Figure 5g). These signal spikes were considered indicative of HER2-positive droplets, and their occurrence was summarized in Figure 5h. These results further supported the efficacy of our platform for accurate screening HER2-positive exosomes in low mixing ratio. Moreover, the screening ability of our SERS-based microdroplet platform against different types of cancerous droplets was also evaluated by mixing droplets containing SKBR3 exosome and MCF-7 exosome at a ratio of 5% to 95% (Figure 5i). Four spike signals were detected after 100 droplet measurements, indicating that our SERS-droplet microfluidic platform holds potential for differentiating HER2-positive tumors from HER2-negative tumors among breast cancer patients. Additionally, the high-throughput capability of our microfluidic chip allowed for the rapid screening of hundreds of droplets per minute, making it suitable for large-scale clinical diagnostics.

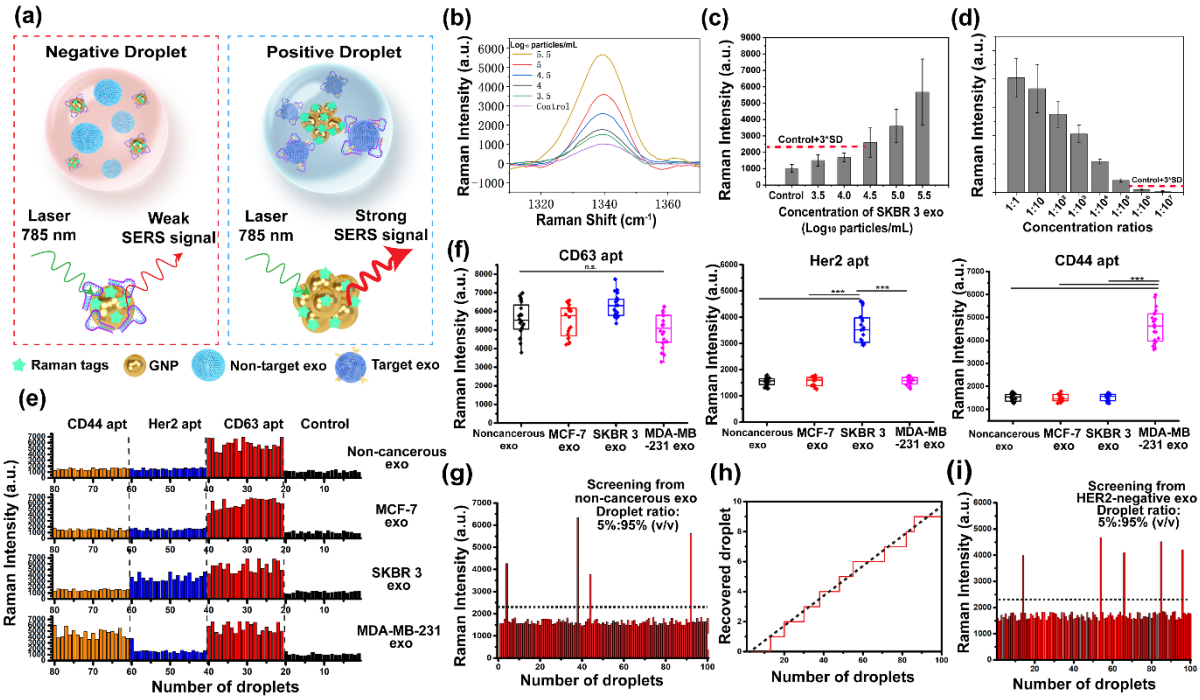

Figure 5. The SERS-based microdroplet platform for detection of Her2-positive exosome extracted from the cell lines. (a) Schematic representation of positive and negative droplets containing SERS-based aptasensors in the presence or absence of Her2-positive exosomes, respectively. (b) The DTNB-SERS spectra were collected from positive droplets containing different concentrations of SKBR3 exosomes (from 3.5 to 5.5 $\log_{10}$ particles/mL) on the chip. (c) The corresponding DTNB-peak intensity was collected from the increasing concentration of SKBR3 exosome. (d) The SERS-based microdroplet platform for detecting HER2-positive exosomes from biomimetic samples. (e) Different exosomes (e.g., non-cancerous, MCF-7, SKBR3, and MDA-MB-231 exos) detection in droplets using different aptamers (e.g., CD 63, HER2, and CD 44 aptamers). The DTNB-peak intensities were measured every 20 droplets. (f) The corresponding quantitative analysis of the collected DTNB-peak intensities from droplets. The DTNB peak intensities of 100 random droplets containing the aptasensor with SKBR3 exosomes and non-cancerous exosomes (g) or SKBR3 exosomes and Her2-negative exosomes (i) were analyzed. The mixing ratio of the two types of droplets was 5% SKBR3 exosomes and 95% non-cancerous exosomes or HER2-negative exosomes, respectively. (h) The corresponding recovery curve of HER2 apt/SKBR3 exo droplets and Her 2 apt/ non-cancerous exo droplets mixed in 5%:95% v/v.

SERS-droplet Microfluidic Platform for Detection of HER2-positive Exosomes in the Clinical Samples

We further evaluate the diagnostic ability of the developed SERS-droplet microfluidic platform for the detection of HER2-positive exosomes in the plasma clinical samples from HER2-positive breast cancer patients. From the SERS spectra, the amplitude of the characteristic DTNB-SERS peak at 1339 cm^{-1} for HER2-positive breast cancer patients was significantly higher than those of the HER2-negative breast cancer patient and the healthy subject (Figure 6a). In fact, the concentration of HER2-positive exosomes extracted from the plasma of HER2-positive breast cancer patients was measured to be around 9.2 log_{10} particles/mL using nano-flow cytometry (Figure S11), which was significantly higher than the LOD around 4.5 log_{10} particles/mL of this SERS-droplet microfluidic platform for detection of HER2-positive exosomes. This demonstrated the diagnostic ability of this platform for clinical samples. Clinically, any patient who is diagnosed with breast cancer should be tested for HER2 status because the results significantly impact treatment recommendations.[41] To study the detection reliability of differentiating HER2-positive patients from HER2-negative breast patients, we analyzed the exosomes based on the SERS spectra from 5 HER2-positive breast patients (n=5) and 5 HER2-negative breast cancer patients (n=5) randomly chosen from the Third Affiliated Hospital of Sun Yat-sen University, Guangzhou, China. The DTNB-SERS peak intensities for samples from all HER2-negative breast cancer patients were markedly lower than those of HER2-positive breast cancer patients (Figure 6b), which was consistent with the clinical diagnosis results. Subsequently, Principal Components Analysis (PCA) was performed on the samples grouped for differential comparison, revealing distinct profiles between HER2-positive breast patient and HER2-negative breast cancer patient groups (Figure 6c). The above results demonstrated the reliability of this platform for HER2 status testing in clinical samples.

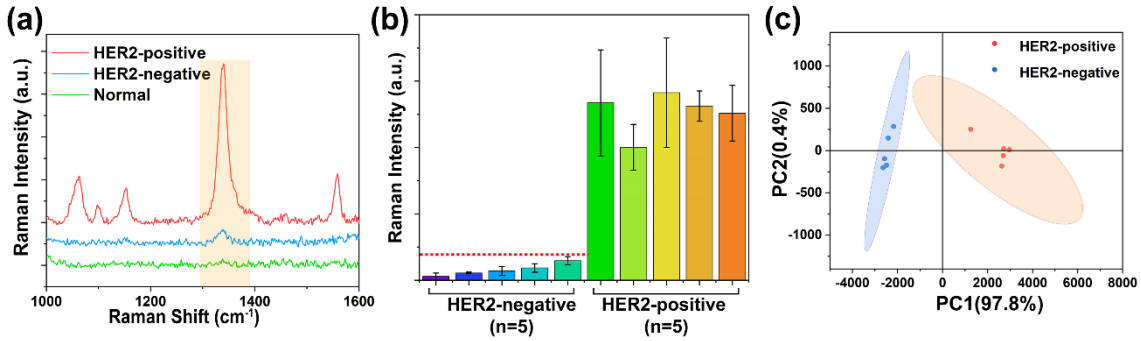

Figure 6. The SERS-based microdroplet platform for the detection of HER2-positive exosomes extracted from plasma in the clinic. (a) The SERS spectra of the aptasensor in the presence of exosomes extracted from healthy individuals, HER2-positive, and Her2-negative patients. (b) Analysis of DTNB-SERS spectra collected from Her2-negative patients (n=5) and Her2-positive patients (n=5). (c) PCA of SERS spectra. The data were classified using 95%

confidence ellipses. The differences in the data were analyzed by PC1 and PC2 (accounting for 97.8% and 0.4% of the variance, respectively), accounting for 98.2% of the total variance.

Conclusion

In this project, we developed a rapid and sensitive SERS-droplet microfluidic platform for the detection of HER2-positive exosomes in both cell lines and clinical samples. By using the on-chip salt-induced GNP aggregation and Raman tag labeling process, this platform achieved a remarkable LOD of 4.5 $\log_{10}$ particles/mL with a sample-to-result time of 5 minutes per sample. In addition, our platform has been successfully applied to test HER2 status in clinical samples, effectively distinguishing HER2-positive and HER2-negative breast cancer patients. However, the significance of our study extends beyond breast cancer diagnostics. The developed SERS-droplet microfluidic platform can be used to detect various cancer-specific exosomal biomarkers, providing a promising approach for non-invasive cancer diagnosis.

Supporting Information

Supporting Information Available: The following files are available free of charge.

Supporting information

Experimental section, TEM images, zeta potential analysis, photographs of droplet generation processes, Raman spectra and Raman intensity analysis, and nano-flow cytometry analysis of SKBR3 exosomes and clinical samples.

Author information

Corresponding Authors

Kunpeng Hu - Department of Breast and Thyroid Surgery, Lingnan Hospital, The Third Affiliated Hospital of Sun Yat-sen University, Guangzhou 510630, China. Email: hukpeng@mail.sysu.edu.cn;

Jingyu Shi - Department of Biomedical Engineering, The Hong Kong Polytechnic University, Kowloon, Hong Kong 999077, China https://orcid.org/0000-0001-7650-8212; Email: jing-yu.shi@polyu.edu.hk;

Mo Yang - Department of Biomedical Engineering, The Hong Kong Polytechnic University, Kowloon, Hong Kong 999077, China; The Hong Kong Polytechnic University Shenzhen Research Institute, Shenzhen 518000, China; Joint Research Center of Biosensing and Precision Theranostics, The Hong Kong Polytechnic University, Kowloon, Hong Kong 999077, China; Research Centre for Nanoscience and Nanotechnology, The Hong Kong

Polytechnic University, Kowloon, Hong Kong 999077, China; https://orcid.org/0000-0002-3863-8187; Email: Mo.Yang@polyu.edu.hk

Authors

Kwun Hei Willis Ho - Department of Biomedical Engineering, The Hong Kong Polytechnic University, Kowloon, Hong Kong 999077, China; Email: kwun-hei-willis.ho@connect.polyu.hk

Huang Lai - Department of Biomedical Engineering, The Hong Kong Polytechnic University, Kowloon, Hong Kong 999077, China; Email: 22108406r@connect.polyu.hk

Ruolin Zhang - Department of Biomedical Engineering, The Hong Kong Polytechnic University, Kowloon, Hong Kong 999077, China; Email: ruolin.zhang@polyu.edu.hk

Haitian Chen - Department of Hepatic Surgery and Liver Transplantation Center of The Third Affiliated Hospital of Sun Yat-sen University, Guangzhou 510630, China; Organ Transplantation Research Center of Guangdong Province, Guangdong Province Engineering Laboratory for Transplantation Medicine; Guangzhou, 510630, China; Email: chenht3@mail2.sysu.edu.cn

Wen Yin - Department of Biomedical Engineering, The Hong Kong Polytechnic University, Kowloon, Hong Kong 999077, China; Email: wen-bme.yin@polyu.edu.hk

Xijing Yan - Department of Breast and Thyroid Surgery, Lingnan Hospital, The Third Affiliated Hospital of Sun Yat-sen University, Guangzhou 510630, China; Email: yanxj7@mail3.sysu.edu.cn

Shu Xiao - Department of Biomedical Engineering, The Hong Kong Polytechnic University, Kowloon, Hong Kong 999077, China; Email: shu.xiao@polyu.edu.hk

Ching Ying Katherine Lam - Department of Biomedical Engineering, The Hong Kong Polytechnic University, Kowloon, Hong Kong 999077, China; https://orcid.org/0000-0002-1207-212X; Email: katherine009.lam@connect.polyu.hk

Yutian Gu - Department of Biomedical Engineering, The Hong Kong Polytechnic University, Kowloon, Hong Kong 999077, China; Email: 20032597r@connect.polyu.hk

JiaXiang Yan - Department of Biomedical Engineering, The Hong Kong Polytechnic University, Kowloon, Hong Kong 999077, China; Email: bryson.yan@connect.polyu.hk

Author Contributions

K.H.W.H. and H.L. contributed equally to this work.

Notes

The authors declare no competing financial interest.

Acknowledgments

This work was supported by the Shenzhen Science and Technology Program-Basic Research Scheme (JCYJ20220531090808020), the Hong Kong Research Grants Council (RGC) Collaborative Research Fund (C5005-23W and C5078-21E), the Research Grants Council (RGC) Hong Kong General Research Fund (15217621 and 15216622), the Guangdong-Hong Kong Technology Cooperation Funding Scheme (GHP/032/20SZ and SGDX20201103095404018), the Hong Kong Polytechnic University Internal Fund (1-YWB4, 1-WZ4E, 1-CD8M, 1-WZ4E, 1-CEB1, 1-YWDU, 1-CE2J and 1-W02C).

References

(1) Zaborowski, M. P.; Balaj, L.; Breakefield, X. O.; Lai, C. P. Extracellular Vesicles: Composition, Biological Relevance, and Methods of Study. Bioscience 2015, 65 (8), 783–797.

(2) Yáñez-Mó, M.; Siljander, P. R. M.; Andreu, Z.; Zavec, A. B.; Borràs, F. E.; Buzas, E. I.; Buzas, K.; Casal, E.; Cappello, F.; Carvalho, J.; Colás, E.; Cordeiro-Da Silva, A.; Fais, S.; Falcon-Perez, J. M.; Ghobrial, I. M.; Giebel, B.; Gimona, M.; Graner, M.; Gursel, I.; Gursel, M.; Heegaard, N. H. H.; Hendrix, A.; Kierulf, P.; Kokubun, K.; Kosanovic, M.; Kralj-Iglic, V.; Krämer-Albers, E. M.; Laitinen, S.; Lässer, C.; Lener, T.; Ligeti, E.; Line, A.; Lipps, G.; Llorente, A.; Lötvall, J.; Manček-Keber, M.; Marcilla, A.; Mittelbrunn, M.; Nazarenko, I.; Nolte-'t Hoen, E. N. M.; Nyman, T. A.; O'Driscoll, L.; Olivan, M.; Oliveira, C.; Pállinger, É.; Del Portillo, H. A.; Reventós, J.; Rigau, M.; Rohde, E.; Sammar, M.; Sánchez-Madrid, F.; Santarém, N.; Schallmoser, K.; Ostenfeld, M. S.; Stoorvogel, W.; Stukelj, R.; Van Der Grein, S. G.; Helena Vasconcelos, M.; Wauben, M. H. M.; De Wever, O. Biological Properties of Extracellular Vesicles and Their Physiological Functions. J. Extracell. Vesicles 2015, 4 (2015), 1–60.

(3) Jiang, L.; Gu, Y.; Du, Y.; Liu, J. Exosomes: Diagnostic Biomarkers and Therapeutic Delivery Vehicles for Cancer. Mol. Pharm. 2019, 16 (8), 3333–3349.

(4) Yu, W.; Hurley, J.; Roberts, D.; Chakrabortty, S. K.; Enderle, D.; Noerholm, M.; Breakefield, X. O.; Skog, J. K. Exosome-Based Liquid Biopsies in Cancer: Opportunities and Challenges. Ann. Oncol. 2021, 32 (4), 466–477.

(5) Li, Q.; Lv, M.; Lv, L.; Cao, N.; Zhao, A.; Chen, J.; Tang, X.; Luo, R.; Yu, S.; Zhou, Y.; Cui, Y.; Guo, W.; Liu, T. Identifying HER2 from Serum-Derived Exosomes in Advanced

Gastric Cancer as a Promising Biomarker for Assessing Tissue HER2 Status and Predicting the Efficacy of Trastuzumab-Based Therapy. Cancer Med. 2023, 12 (4), 4110–4124.
(6) Ciravolo, V.; Huber, V.; Ghedini, G. C.; Venturelli, E.; Bianchi, F.; Campiglio, M.; Morelli, D.; Villa, A.; Mina, P. Della; Menard, S.; Filipazzi, P.; Rivoltini, L.; Tagliabue, E.; Pupa, S. M. Potential Role of HER2-Overexpressing Exosomes in Countering Trastuzumab-Based Therapy. J. Cell. Physiol. 2012, 227 (2), 658–667.
(7) Runz, S.; Keller, S.; Rupp, C.; Stoeck, A.; Issa, Y.; Koensgen, D.; Mustea, A.; Sehouli, J.; Kristiansen, G.; Altevogt, P. Malignant Ascites-Derived Exosomes of Ovarian Carcinoma Patients Contain CD24 and EpCAM. Gynecol. Oncol. 2007, 107 (3), 563–571.
(8) Amrollahi, P.; Rodrigues, M.; Lyon, C. J.; Goel, A.; Han, H.; Hu, T. Y. Ultra-Sensitive Automated Profiling of EpCAM Expression on Tumor-Derived Extracellular Vesicles. Front. Genet. 2019, 10, 1–10.
(9) Cheng, Y.; Xie, Q.; He, M.; Chen, B.; Chen, G.; Yin, X.; Kang, Q.; Xu, Y.; Hu, B. Sensitive Detection of Exosomes by Gold Nanoparticles Labeling Inductively Coupled Plasma Mass Spectrometry Based on Cholesterol Recognition and Rolling Circle Amplification. Anal. Chim. Acta 2022, 1212 (May), 339938.
(10) Logozzi, M.; Di Raimo, R.; Mizzoni, D.; Fais, S. Immunocapture-Based ELISA to Characterize and Quantify Exosomes in Both Cell Culture Supernatants and Body Fluids, Methods in enzymology 2020, 645, 155-180.
(11) Khodashenas, S.; Khalili, S.; Forouzandeh Moghadam, M. A Cell ELISA Based Method for Exosome Detection in Diagnostic and Therapeutic Applications. Biotechnol. Lett. 2019, 41 (4–5), 523–531.
(12) Theodoraki, M. N.; Hong, C. S.; Donnenberg, V. S.; Donnenberg, A. D.; Whiteside, T. L. Evaluation of Exosome Proteins by On-Bead Flow Cytometry. Cytom. Part A 2021, 99 (4), 372–381.
(13) Huang, R.; He, L.; Li, S.; Liu, H.; Jin, L.; Chen, Z.; Zhao, Y.; Li, Z.; Deng, Y.; He, N. A Simple Fluorescence Aptasensor for Gastric Cancer Exosome Detection Based on Branched Rolling Circle Amplification. Nanoscale 2020, 12 (4), 2445–2451.
(14) Yoshioka, Y.; Kosaka, N.; Konishi, Y.; Ohta, H.; Okamoto, H.; Sonoda, H.; Nonaka, R.; Yamamoto, H.; Ishii, H.; Mori, M.; Furuta, K.; Nakajima, T.; Hayashi, H.; Sugisaki, H.; Higashimoto, H.; Kato, T.; Takeshita, F.; Ochiya, T. Ultra-Sensitive Liquid Biopsy of Circulating Extracellular Vesicles Using ExoScreen. Nat. Commun. 2014, 5, 3591.

(15) Xu, L.; Chopdat, R.; Li, D.; Al-Jamal, K. T. Development of a Simple, Sensitive and Selective Colorimetric Aptasensor for the Detection of Cancer-Derived Exosomes. Biosens. Bioelectron. 2020, 169, 112576.
(16) Wang, S.; Zhang, L.; Wan, S.; Cansiz, S.; Cui, C.; Liu, Y.; Cai, R.; Hong, C.; Teng, I. T.; Shi, M.; Wu, Y.; Dong, Y.; Tan, W. Aptasensor with Expanded Nucleotide Using DNA Nanotetrahedra for Electrochemical Detection of Cancerous Exosomes. ACS Nano 2017, 11 (4), 3943–3949.
(17) Dong, H.; Chen, H.; Jiang, J.; Zhang, H.; Cai, C.; Shen, Q. Highly Sensitive Electrochemical Detection of Tumor Exosomes Based on Aptamer Recognition-Induced Multi-DNA Release and Cyclic Enzymatic Amplification. Anal. Chem. 2018, 90 (7), 4507–4513.
(18) An, J.; Park, H.; Kim, J.; Park, H.; Kim, T. H.; Park, C.; Kim, J.; Lee, M. H.; Lee, T. Extended-Gate Field-Effect Transistor Consisted of a CD9 Aptamer and MXene for Exosome Detection in Human Serum. ACS Sensors 2023, 8 (8), 3174–3186.
(19) McNay, G.; Eustace, D.; Smith, W. E.; Faulds, K.; Graham, D. Surface-Enhanced Raman Scattering (SERS) and Surface-Enhanced Resonance Raman Scattering (SERRS): A Review of Applications. Appl. Spectrosc. 2011, 65 (8), 825–837.
(20) Shin, H.; Jeong, H.; Park, J.; Hong, S.; Choi, Y. Correlation between Cancerous Exosomes and Protein Markers Based on Surface-Enhanced Raman Spectroscopy (SERS) and Principal Component Analysis (PCA). ACS Sensors 2018, 3 (12), 2637–2643.
(21) Yin, B.; Ho, W. K. H.; Xia, X.; Chan, C. K. W.; Zhang, Q.; Ng, Y. M.; Lam, C. Y. K.; Cheung, J. C. W.; Wang, J.; Yang, M.; Wong, S. H. D. A Multilayered Mesoporous Gold Nanoarchitecture for Ultraeffective Near-Infrared Light-Controlled Chemo/Photothermal Therapy for Cancer Guided by SERS Imaging. Small 2023, 19 (6), 1–14.
(22) Dong, S.; Wang, Y.; Liu, Z.; Zhang, W.; Yi, K.; Zhang, X.; Zhang, X.; Jiang, C.; Yang, S.; Wang, F.; Xiao, X. Beehive-Inspired Macroporous SERS Probe for Cancer Detection through Capturing and Analyzing Exosomes in Plasma. ACS Appl. Mater. Interfaces 2020, 12 (4), 5136–5146.
(23) Shin, H.; Oh, S.; Hong, S.; Kang, M.; Kang, D.; Ji, Y. G.; Choi, B. H.; Kang, K. W.; Jeong, H.; Park, Y.; Kim, H. K.; Choi, Y. Early-Stage Lung Cancer Diagnosis by Deep Learning-Based Spectroscopic Analysis of Circulating Exosomes. ACS Nano 2020, 14 (5), 5435–5444.
(24) Yin, B.; Zhang, Q.; Xia, X.; Li, C.; Ho, W. K. H.; Yan, J.; Huang, Y.; Wu, H.; Wang, P.; Yi, C.; Hao, J.; Wang, J.; Chen, H.; Wong, S. H. D.; Yang, M. A CRISPR-Cas12a

Integrated SERS Nanoplatform with Chimeric DNA/RNA Hairpin Guide for Ultrasensitive Nucleic Acid Detection. Theranostics 2022, 12 (13), 5914–5930.
(25) Wang, Z.; Zong, S.; Wang, Y.; Li, N.; Li, L.; Lu, J.; Wang, Z.; Chen, B.; Cui, Y. Screening and Multiple Detection of Cancer Exosomes Using an SERS-Based Method. Nanoscale 2018, 10 (19), 9053–9062.
(26) Tian, Y. F.; Ning, C. F.; He, F.; Yin, B. C.; Ye, B. C. Highly Sensitive Detection of Exosomes by SERS Using Gold Nanostar@Raman Reporter@nanoshell Structures Modified with a Bivalent Cholesterol-Labeled DNA Anchor. Analyst 2018, 143 (20), 4915–4922.
(27) Balčytis, A.; Nishijima, Y.; Krishnamoorthy, S.; Kuchmizhak, A.; Stoddart, P. R.; Petruškevičius, R.; Juodkazis, S. From Fundamental toward Applied SERS: Shared Principles and Divergent Approaches. Adv. Opt. Mater. 2018, 6 (16), 1–29.
(28) Shi, J., Zhang, Y., & Yang, M. Recent development of microfluidics-based platforms for respiratory virus detection. Biomicrofluidics 2023, 17(2).
(29) Chen, J.; Oudeng, G.; Feng, H.; Liu, S.; Li, H. W.; Ho, Y. P.; Chen, Y.; Tan, Y.; Yang, M. 2D MOF Nanosensor-Integrated Digital Droplet Microfluidic Flow Cytometry for In Situ Detection of Multiple MiRNAs in Single CTC Cells. Small 2022, 18 (32), 1–13.
(30) Shi, J.; Zhang, Y.; Fan, Y.; Liu, Y.; Yang, M. Recent Advances in Droplet-Based Microfluidics in Liquid Biopsy for Cancer Diagnosis. Droplet 2024, 3 (1).
(31) Yue, S.; Fang, J.; Xu, Z. Advances in Droplet Microfluidics for SERS and Raman Analysis. Biosens. Bioelectron. 2022, 198, 113822.
(32) Gao, R.; Cheng, Z.; Wang, X.; Yu, L.; Guo, Z.; Zhao, G.; Choo, J. Simultaneous Immunoassays of Dual Prostate Cancer Markers Using a SERS-Based Microdroplet Channel. Biosens. Bioelectron. 2018, 119, 126–133.
(33) Park, S.; Su Jeon, C.; Choi, N.; Moon, J. Il; Min Lee, K.; Hyun Pyun, S.; Kang, T.; Choo, J. Sensitive and Reproducible Detection of SARS-CoV-2 Using SERS-Based Microdroplet Sensor. Chem. Eng. J. 2022, 446, 137085.
(34) Choi, N.; Lee, J.; Ko, J.; Jeon, J. H.; Rhie, G. E.; DeMello, A. J.; Choo, J. Integrated SERS-Based Microdroplet Platform for the Automated Immunoassay of F1 Antigens in Yersinia Pestis. Anal. Chem. 2017, 89 (16), 8413–8420.
(35) Cong, L.; Wang, J.; Li, X.; Tian, Y.; Xu, S.; Liang, C.; Xu, W.; Wang, W.; Xu, S. Microfluidic Droplet-SERS Platform for Single-Cell Cytokine Analysis via a Cell Surface Bioconjugation Strategy. Anal. Chem. 2022, 94 (29), 10375–10383.
(36) Lv, M. M.; Zhu, X. Y.; Chen, W. X.; Zhong, S. L.; Hu, Q.; Ma, T. F.; Zhang, J.; Chen, L.; Tang, J. H.; Zhao, J. H.; Exosomes mediate drug resistance transfer in MCF-7 breast

cancer cells and a probable mechanism is delivery of P-glycoprotein. Tumor Biol. 2014, 35, 10773–10779.

(37) Li, H.; Rothberg, L. Colorimetric Detection of DNA Sequences Based on Electrostatic Interactions with Unmodified Gold Nanoparticles. Proc. Natl. Acad. Sci. U. S. A. 2004, 101 (39), 14036–14039.

(38) Ding, S. Y.; You, E. M.; Tian, Z. Q.; Moskovits, M. Electromagnetic Theories of Surface-Enhanced Raman Spectroscopy. Chem. Soc. Rev. 2017, 46 (13), 4042–4076.

(39) Yin, B.; Ho, W. K. H.; Zhang, Q.; Li, C.; Huang, Y.; Yan, J.; Yang, H.; Hao, J.; Wong, S. H. D.; Yang, M. Magnetic-Responsive Surface-Enhanced Raman Scattering Platform with Tunable Hot Spot for Ultrasensitive Virus Nucleic Acid Detection. ACS Appl. Mater. Interfaces 2022, 14 (3), 4714–4724.

(40) Song, D.; Yang, R.; Fang, S.; Liu, Y.; Long, F.; Zhu, A. SERS Based Aptasensor for Ochratoxin A by Combining Fe3O4@Au Magnetic Nanoparticles and Au-DTNB@Ag Nanoprobes with Multiple Signal Enhancement. Microchim. Acta 2018, 185, 1-10.

(41) Wolff, A. C.; Hammond, M. E. H.; Allison, K. H.; et al. Human Epidermal Growth Factor Receptor 2 Testing in Breast Cancer: American Society of Clinical Oncology/College of American Pathologists Clinical Practice Guideline Focused Update. *J. Clin. Oncol.* 2018, *36* (20), 2105-2122.

(42) Bastús, N. G.; Comenge, J.; Puntes, V. Kinetically Controlled Seeded Growth Synthesis of Citrate-Stabilized Gold Nanoparticles of up to 200 Nm: Size Focusing versus Ostwald Ripening. Langmuir 2011, 27 (17), 11098–11105.

(43) Johnson, P. B., & Christy, R. W. Optical constants of the noble metals. Physical review B 1972, 6(12), 4370.

For Table of contents